XLVI CILAMCE
VITÓRIA - ES - BRAZIL - 2025
XLVI IBERO-LATIN AMERICAN CONGRESS ON COMPUTATIONAL METHODS IN ENGINEERING

Trajectory Control of a 6×6 Vehicle for Driver Assistance

Camila L. Pereira.[1], Ricardo T. C. Neto[1]

[1]*Dept. of Mechanical Engineering, Military Institute of Engineering*
Praça Gen. Tibúrcio, 80, 22290-270, Rio de Janeiro/RJ, Brazil
camilaleao@ime.eb.br, ricardo@ime.eb.br

Abstract. Military vehicles operating on uneven terrain are susceptible to rollovers during abrupt maneuvers, motivating the development of advanced driver-assistance systems to enhance safety and stability. This study presents trajectory-tracking controllers based on a 2-DOF SHM model of the Guarani combat vehicle in MATLAB®, using front wheel steering modulation via LQR and MPC. Simulation results from slalom and turning radius maneuvers, including open-loop comparisons, show that both controllers achieve accurate path tracking while maintaining stability, highlighting that MPC exhibits notably smoother control actions, with the MPC providing smoother control actions, which is advantageous for real-time implementation.

Keywords: LQR controller, MPC controller, Path Tracking, Vehicle Dynamics, Wheeled Military Vehicles.

1 Introduction

The 6×6 Guarani Armored Personnel Carrier (APC), employed by the Brazilian Army, exhibits dynamic features such as a high center of gravity and large moments of inertia, which can compromise its stability and require advanced driver skills and experience. Reported rollover incidents between 2017 and 2020 have motivated studies focused on enhancing vehicle safety through driver assistance and stability control systems, aligned with the broader trend toward progressive automation in military and civilian vehicles.

This study proposes a computational dynamic model of a 6x6 vehicle based on a Simple Handling Model (SHM), also referred to as a single-track or bicycle model, integrated with Linear Quadratic Regulator (LQR) and Model Predictive Control (MPC) strategies. The objective is to enhance the vehicle's maneuverability, stability, and dynamic response, without directly addressing the rollover phenomena. By regulating yaw rate and lateral velocity, the controllers contribute to maintaining directional stability and minimizing trajectory tracking errors [1]. Moreover, while kinematic models are suitable for low speed applications, incorporating dynamic effects is essential for realistic simulations and for validating advanced control strategies [2].

Although LQR and MPC are well-established in civilian automotive research, studies focused on military heavy vehicles remain scarce. These vehicles pose unique challenges due to their higher mass and inertia, slower response, and operation on uneven terrain. In related research, Acuña et al. [3] used a SHM model of a 6×6 military truck and an adaptive MPC controller was applied to reproduce driver behavior in a NATO double lane-change test, and results were validated against a high-fidelity TruckSim® model. Similarly, Deng et al. [4] developed an LQR-based active steering strategy for articulated heavy vehicles, validated through MATLAB®/TruckSim® simulations and hardware-in-the-loop (HIL) tests, demonstrating improved maneuverability and stability in demanding maneuvers.

Song et al. [5] employed an LQR controller optimized by a genetic algorithm for a 2-DOF truck model, achieving improved path-tracking precision under parameter uncertainties. Zhang et al. [6] compared MPC, Pure Pursuit, and LQR algorithms for intelligent vehicles in MATLAB®, reporting that MPC provides higher accuracy while LQR offers faster computation and better real-time performance. Both controllers demonstrated stable

behavior across varying speeds, highlighting their suitability for dynamic path tracking. Other studies have applied MPC and LQR to multi-axle and articulated vehicles. For instance, Liu et al. [7] proposed an MPC-based trajectory planner incorporating sideslip and yaw rate constraints, enhancing safety during high-speed obstacle avoidance.

Despite these advances, applications of such control strategies to 6×6 military vehicles, with their specific geometry, load distribution, and dynamic constraints, remain limited. This work addresses that gap by developing and simulating on MATLAB®/Simulink® a trajectory-following controller for the Guarani APC using LQR and MPC approaches based on an SHM representation, incorporating estimated parameters from experimental field data. The results provide comparative insights into performance and control smoothness for potential future applications.

2 Simple Handling Vehicle Model – SHM

A body-fixed coordinate system Cxyz (point C denoting the vehicle's center of mass) is defined to an inertial reference frame OXYZ (Fig. 1). The vehicle's orientation is expressed through the roll (φ), pitch (θ), and yaw (ψ) angles. The time derivatives of these angles, known respectively as roll rate ($\dot{\varphi}$), pitch rate ($\dot{\theta}$), and yaw rate ($\dot{\psi}$), constitute fundamental dynamic variables [8]. According to Jazar [8], when longitudinal, lateral, and angular velocities are sufficient to capture the primary vehicle dynamics, a planar model is considered appropriate.

For the tracking trajectory study, the proposed approach adopts a simplified lateral dynamics model. The SHM (Fig. 2) is widely used in control system design due to its simplicity and computational efficiency. In this formulation, the wheels on each axle are represented by a single equivalent wheel, which consolidates the tire-road interaction forces. Under these assumptions, the vehicle is modeled as a rigid body with three degrees of freedom: translational motion along the x and y axes, and rotational motion about the z axis.

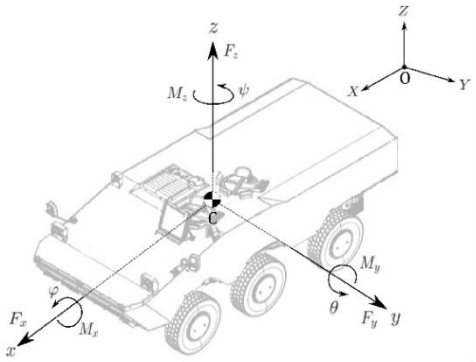


Figure 1. Coordinates of the body-fixed reference frame Cxyz, defined relative to the inertial frame OXYZ, in accordance with ISO 8855

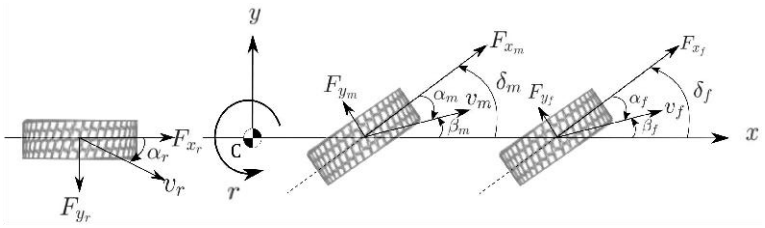


Figure 2. Forces diagram of the SHM

Additionally, in Fig. 2, let α_j denote the slip angle; F_{xj} the longitudinal force; F_{yj} the lateral force; v_j the linear velocity at the contact patch; β_j the sideslip angle; and δ_j the steer angle of tire j, where f, m, and r correspond to the front, middle, and rear axles, respectively. As a simplifying assumption, dynamic load transfer (both longitudinal and lateral) is neglected. For the purposes of controller design, further assumptions include

small-angle approximations, constant longitudinal velocity, and the adoption of a linear tire model. The front and middle axles steer with angles δ_f and δ_m, respectively, while the effects of roll and other dynamic behavior, such as pitch, are disregarded. Considering a constant longitudinal speed v_x, eq. (1) presents a simplified mathematical formulation for the vehicle's lateral dynamics [9], where the longitudinal and the lateral forces applied in the present study are defined by eq. (2) and eq. (3), respectively.

$$\begin{bmatrix}\dot{v}_y \\ \dot{r}\end{bmatrix} = \begin{bmatrix} \frac{sen(\delta_f)}{m} & \frac{cos(\delta_f)}{m} & \frac{sen(\delta_m)}{m} & \frac{cos(\delta_m)}{m} & 0 & \frac{1}{m} \\ \frac{a_1 sen(\delta_f)}{I_{zz}} & \frac{a_1 cos(\delta_f)}{I_{zz}} & \frac{a_1 cos(\delta_f)}{I_{zz}} & \frac{a_2 sen(\delta_m)}{I_{zz}} & 0 & \frac{-a_3}{I_{zz}} \end{bmatrix} \begin{bmatrix} F_{xf} \\ F_{yf} \\ F_{xm} \\ F_{ym} \\ F_{xr} \\ F_{yr} \end{bmatrix} - \begin{bmatrix} r v_x \\ 0 \end{bmatrix} \tag{1}$$

$$F_{xf} = F_{xm} = F_{xr} = \frac{-mrv_y}{3} \tag{2}$$

$$F_{yj} = -C_{\alpha j}(\beta_j - \delta_j) \tag{3}$$

Let m denote the vehicle mass; I_{zz} the moment of inertia about the z-axis; a_1, a_2, and a_3 the distances from the front, middle, and rear axles to the vehicle body's center of mass (C), respectively; while $C_{\alpha j}$ denotes the cornering stiffness of the equivalent tire of the j-axle. Moreover, it is assumed that the steer angle of the middle axle (δ_m) is mechanically linked to that of the front axle (δ_f), as described by eq. (4).

$$\delta_m = [(a_2 + a_3)/(a_1 + a_3)]\delta_f \tag{4}$$

The state variables of interest are the lateral velocity v_y and the yaw rate r, while the system input is the front steer angle δ_f, which serves as the control variable. Based on the previous equations, the linearized state-space representation of the system is given in eq. (5).

$$\begin{bmatrix}\dot{v}_y \\ \dot{r}\end{bmatrix} = \begin{bmatrix} -\left(\frac{C_{\alpha f}+C_{\alpha m}+C_{\alpha r}}{m v_x}\right) & \frac{-a_1 C_{\alpha f} - a_2 C_{\alpha m} + a_3 C_{\alpha r}}{m v_x} - v_x \\ -\frac{a_1 C_{\alpha f} + a_2 C_{\alpha m} - a_3 C_{\alpha r}}{I_{zz} v_x} & -\frac{a_1^2 C_{\alpha f} + a_2^2 C_{\alpha m} + a_3^2 C_{\alpha r}}{I_{zz} v_x} \end{bmatrix} \begin{bmatrix} v_y \\ r \end{bmatrix} + \begin{bmatrix} \frac{C_{\alpha f}}{m} + \left(\frac{a_2+a_3}{a_1+a_3}\right)\frac{C_{\alpha m}}{m} \\ \frac{a_1 C_{\alpha f}}{I_{zz}} + \left(\frac{a_2+a_3}{a_1+a_3}\right)\frac{a_2 C_{\alpha m}}{I_{zz}} \end{bmatrix} \delta_f \tag{5}$$

Although models with constant cornering stiffness can only accurately represent vehicle dynamics during near-steady-state maneuvers, typically associated with lateral accelerations below 0.4 g on asphalt surfaces [10], these values remain suitable for controller design based on linear tire models [11,12] or for applications using linearized model around a nominal operating point [19,18]. Since the cornering stiffness values were not available, they were estimated using the Levenberg–Marquardt parameter estimation method, based on experimental data collected during field tests, after confirming that the expected cornering stiffness values could be recovered from simulated data [9].

As described by Pereira et al. [9], for the field experiments, the APC Guarani was subjected to a double lane-change test at a speed of 10 km/h. Data acquisition was carried out using a Racelogic® VBOX 3i, a Racelogic® IMU RLVBIMU04, and a 500 mm MICRO-EPSILON® LVDT transducer. The IMU provides pitch, roll, and yaw rates, as well as accelerations along the three coordinate axes. A function correlating the transducer voltage with the steering wheel angle was implemented within the VBOX analysis software. Both the IMU and the transducer were connected to the VBOX to log the test data. Post-processing of the recorded measurements was performed using a low-pass filter implemented in MATLAB®. A sensitivity analysis indicated that the cornering stiffness of the middle axle tire has a negligible effect on the yaw rate, compared to other parameters, according to Arndt et al. [10]. Consequently, the estimation procedure focused on the cornering stiffness values of the front and rear axles. The experimental data were sampled at 100 Hz, requiring the Simulink® model to be configured accordingly. The final set of parameter values used in the simulations is summarized in Tab. 1.

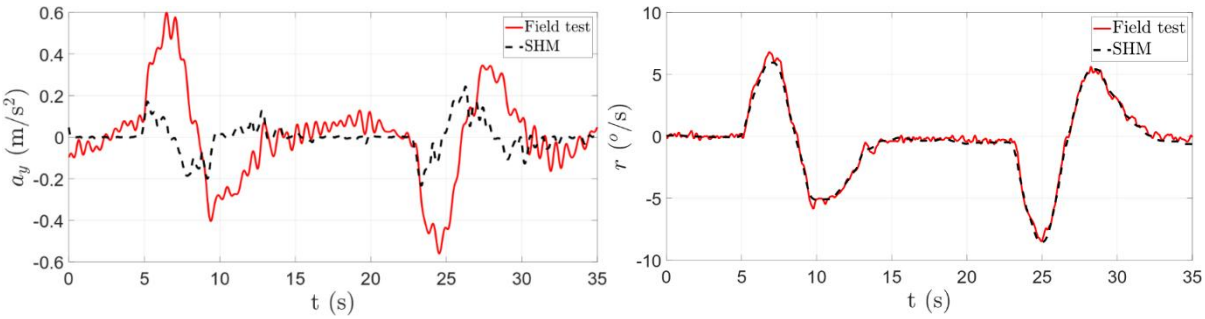
Table 1. Inputs parameters to the estimation process using field data

Input parameters in MATLAB®					
Vehicle mass m	15770 kg	I_{zz}	63595.4 kgm^2	v_x	10 km/h
a_1	1.77 m	a_2	0.07 m	a_3	1.93m
differentiation step	10^{-8}	Initial λ value (*)	10^7	Tolerance	10^{-6}
Max. nr of iterations	1000	$C_{\alpha m}$ (fixed)	300 kN/rad	$C_{\alpha r}$ initial value	300 kN/rad
$C_{\alpha f}$ initial value	300 kN/rad				

(*) Parameter of the Levenberg-Marquardt method

The estimated values for the cornering stiffness were $C_{\alpha f}$ = 222.930 kN/rad and $C_{\alpha r}$= 80.032 kN/rad. These results are consistent with those reported by Luty and Simiński [15], where a 14.00R20 run-flat tire, inflated to 500 kPa and subjected to a vertical load of 2667 kgf, exhibited cornering stiffness values in the range of 130 to 170 kN/rad. Consequently, for the SHM, the equivalent tire cornering stiffness is expected to fall between 260 and 340 kN/rad. Therefore, the estimated value of $C_{\alpha f}$ closely matches the expected range, while $C_{\alpha r}$ is notably lower. This result may be explained by the axle load distribution of the APC Guarani, 35.2% on the front axle, 37.9% on the middle axle, and 26.9% on the rear axle. Assuming that the only difference between the tires lies in the vertical load supported, it is reasonable to expect $C_{\alpha m} > C_{\alpha f} > C_{\alpha r}$. Furthermore, the selected value of $C_{\alpha m}$ influences the estimates of $C_{\alpha f}$ and $C_{\alpha r}$, as an increase in $C_{\alpha m}$ tends to raise $C_{\alpha f}$ and lower $C_{\alpha r}$ [9].

A comparison between the measured and the numerical solution of the yaw rate and lateral acceleration obtained using the estimated parameters from the forward problem is presented in Fig. 3. The numerical results of the yaw rate show good agreement with the actual vehicle response in terms of behavior and magnitude. However, although the experimental and simulated lateral acceleration curves exhibit similar trends, larger discrepancies were observed. Possible sources of these differences include measurement uncertainties and model parameters, as well as unmodeled dynamic effects and external forces not captured by the simplified computational model. It is also important to note that the field test was conducted by a human driver, and the vehicle speed during the experiment varied from 10.4 km/h to 12.3 km/h, while the simulation assumed a constant longitudinal velocity of 10 km/h. The cornering stiffness parameters estimated using the Levenberg–Marquardt method were subsequently incorporated into the SHM to support the design of LQR and MPC controllers.



(a) Lateral acceleration (b) Yaw rate

Figure 3. Comparative experimental data and SHM numerical solution of the yaw rate and lateral acceleration.

3 LQR and MPC controllers

Yaw rate monitoring is recognized as an effective method of maintaining vehicle control without compromising the vehicle's drivability. The desired yaw rate is inferred from the steering wheel input and the vehicle's longitudinal velocity. For this reason, the Linear Quadratic Regulator (LQR) technique is commonly employed in steering control for multi-axle vehicles. LQR is based on the solution of an optimization problem that minimizes a quadratic cost function (objective function) and is extensively used in vehicle trajectory tracking

control. One of its main advantages is that the optimal control signal can be computed via full-state feedback (see Fig. 4).

However, a notable limitation of this approach is its inability to directly incorporate constraints on system or control inputs—such as restricting an actuator's operating range to prevent saturation. As shown in Fig. 4, the system is presented in state-space form for the controller design, where $\boldsymbol{x}$ denotes the state vector; $\boldsymbol{u}$ the control's input vector; and $\boldsymbol{K_{LQR}}$ is the gain matrix applied in the control law. The linearized state-space model, used as the basis for LQR design, was previously expressed by eq. (5).

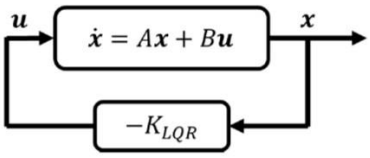


Figure 4. LQR controller scheme

Given these considerations, Model Predictive Control (MPC) has emerged as one of the most widely used optimal control strategies for both nonlinear systems and linear systems with constraints [16]. Its appeal lies in the ability to incorporate state and input constraints directly into the optimization problem through the cost function. MPC has seen widespread application in the automotive domain, especially in safety and driver assistance systems, including trajectory tracking for off-road vehicles.

MPC uses a dynamic model of the system to predict future states and optimize closed-loop control performance over a finite prediction horizon. Although MPC is not inherently robust, it performs reliably when the model accurately represents the system dynamics. Its primary advantage lies in its predictive capability, which allows for anticipatory control actions and improved transient response. Nonetheless, performance may deteriorate in the presence of significant model uncertainties, which conventional (non-robust) MPC does not explicitly address [2]. In this study, based on the SHM framework, the vehicle dynamics were modeled assuming a small steer angle δ_f and constant longitudinal velocity v_x, according to eq. (1). The trajectory of the linearized model, given in eq. (5), was considered as the reference for the control system. Furthermore, the lateral velocity v_y and the yaw rate *r*, both relevant for minimizing lateral deviation from the desired trajectory, were selected as state variables of $\boldsymbol{x}$, while the front steer angle δ_f serves as the control input [17].

3.1 Linear Quadratic Regulator (LQR) control algorithm

Starting from an initial condition in which all state variables are set to zero, Tab. 2 outlines the sequence steps used to solve the formulated control problem, preserving the nonlinearities of the system while employing time-varying A_{LQR} and B_{LQR} matrices based on reference points.

Table 2. LQR algorithm

Inputs	Vehicle and controller parameters, $\boldsymbol{x}(t=0)$, function $\delta_f(t)$
Start	
Step 1	Computation of the reference vector $\boldsymbol{x}_{ref}$ (tracking variables)
Step 2	Computation of the $\mathbf{A}_{\mathrm{LQR}}$ and $\mathbf{B}_{\mathrm{LQR}}$ matrices based on the variables of $\boldsymbol{x}_{ref}$
Step 3	Determination of the optimal gain matrix $\mathbf{K}_{\mathrm{LQR}}$
Step 4	Trajectory correction at each time step *t*, by updating the input $\boldsymbol{u}$ using the control law $\boldsymbol{u}_{control} = \mathbf{K}_{LQR}^{(i-1)} \times \left(\boldsymbol{x}_{ref} - \boldsymbol{x}_{real}\right) + \boldsymbol{u}$, based on the state values from the previous time step.
Step 5	Integration of $\dot{\boldsymbol{x}}_{real}$ to obtain the updated real state $\boldsymbol{x}_{real}$
End	

3.2 Model Predictive Control (MPC) algorithm

The LQR and MPC algorithms share similarities in their quadratic optimization formulation. However, a key difference lies in the prediction horizon: MPC solves the optimization problem over a receding time horizon, whereas LQR does so over a fixed time window. The moving horizon approach enables the controller to adapt to stricter real-time constraints. As described by Durmaz et al. [18], at each sampling instant, only the first control input of the optimized sequence is applied to the system. At the next time step, a new optimal control problem is solved to determine the subsequent control signal. Among the main advantages of predictive control over other methods are coordination of multiple inputs and outputs in arbitrary models (linear and nonlinear); performance optimization while accounting for system, state, input, and process constraints; and use of future state predictions based on a mathematical model, which enhances the system's ability to reach the desired target more efficiently [18].

For the computational implementation of the MPC controller, the multiple shooting method was adopted for model discretization, as it is well-suited for nonlinear systems as pointed out by Sánchez et al. [19]. In this approach, the system states are treated as decision variables. The algorithm presented in Tab.3 describes the sequence of steps executed by the controller to compute the optimal control inputs, minimizing the tracking error between the simulated and reference trajectories, and consequently, thereby enhancing the accuracy of the control system.

Table 3. MPC algorithm

Inputs	Vehicle and controller parameters, $\boldsymbol{x}(t=0)$, function $\delta_f(t)$, systems constraints
Start	
Repeat...	
Step 1	Acquisition of the updated state vector $\boldsymbol{x}(t)$
Step 2	Solution of the optimization problem with respect to the control inputs $(u_0, \cdots, u_{N-1})$
Step 3	Application of only the first optimal input value $u(t) = u_0^* = u_k^*$ to the system, while the remaining inputs in the sequence are disregarded
Until...	t(s) = end simulation time
End	

MPC supports a multivariable control framework and directly incorporates constraints into the objective function. Consequently, the optimization problem becomes more complex, especially when aiming for real-time implementation [20]. Given the significantly greater computational complexity compared to LQR, the CasADi® framework was employed to symbolically formulate and solve the optimization problem.

4 Results and Discussion

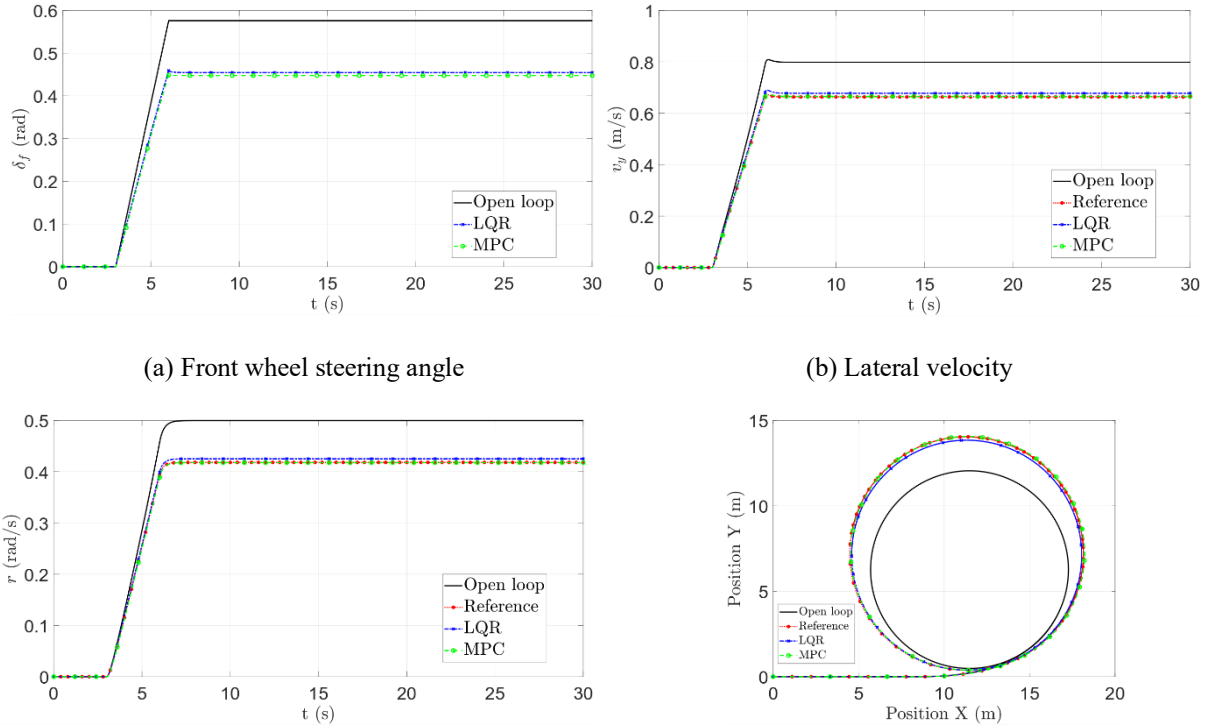
The model described by eq. (1) was evaluated under two standard dynamic tests: a turning- radius (i.e., a sudden ramp input) and a slalom maneuver (i.e., sinusoidal input). These tests are commonly used to assess lateral stability and trajectory-following performance. The parameters used in the simulations were drawn from Tab. 1. The reference vector $\boldsymbol{x}_{ref}$ was computed using the linearized equations of motion, described by eq. (5), to generate the reference trajectory. To assess the controllers' effectiveness, a 10% increase in the steering input was introduced to emulate a realistic disturbance scenario. The simulation results are shown in Fig. 5 and Fig. 6, while the Root-Mean-Square-Error (RMSE) of the state variables are summarized in Tab. 4, including comparisons with the open-loop system's behavior.

In the absence of a control system (open-loop configuration), the vehicle follows a trajectory solely determined by the steering input signal, resulting in significant deviations from the desired path. When the control laws are applied, despite the intentional 10% disturbance in steering input, both controllers effectively minimize

the tracking errors in the lateral velocity and yaw rate (Fig. 5(b), Fig. 5(c), Fig. 6(b) and Fig. 6(c)), guiding the vehicle back toward the reference path. As observed in the turning radius maneuver, the controlled systems initially follow the open-loop behavior until corrective action becomes necessary after the step input is applied. From that point onward, both controllers adjust the steering angle to maintain the desired trajectory.

Table 4. Comparative RMSE of the open-loop and the controlled systems response.

Turning	**Open-loop**	**LQR**	**MPC**	**Slalom**	**Open-loop**	**LQR**	**MPC**
RMSE v_y	0.1219	0.0129	0.0022	RMSE v_y	0.0634	0.0069	0.0028
RMSE r	0.0734	0.0064	0.0012	RMSE r	0.0388	0.0037	0.0021



(a) Front wheel steering angle

(b) Lateral velocity

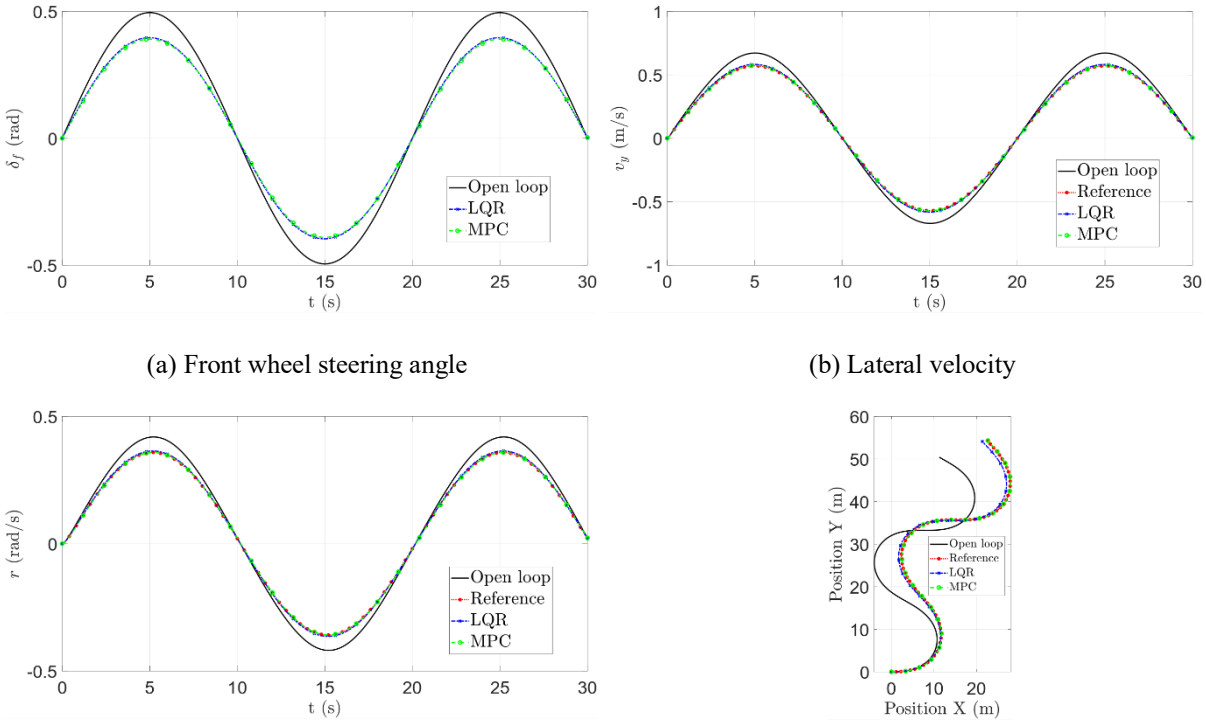
(c) Yaw rate

(d) XY trajectory for a turning maneuver

Figure 5. Results with and without the integration of LQR and MPC controllers for a turning radius maneuver.

A noticeable distinction between the two control strategies appears in the control input response (front steering angle, Fig. 5(a)) and in the lateral velocity (Fig. 5(b)). The LQR exhibits a higher transient peak after the ramp input, whereas the MPC response is smoother. This smoother behavior arises from the predictive optimization mechanism of MPC, which minimizes not only the tracking error, but also the control effort over a prediction horizon. By incorporating constraints and weighting terms on the rate of change of the control input (aligned with predictions of the vehicle's future behavior) MPC inherently penalizes abrupt steering actions, leading to reduced actuator demand and less oscillatory motion. In contrast, LQR generates instantaneous optimal control based solely on the current state, which may result in faster but more aggressive corrections.

The practical implications of the smoother MPC response are relevant for both comfort and vehicle handling in real-world applications. Smoother steering commands reduce mechanical stress of vehicle components, extending component life and lowering energy consumption. From a driver-assistance perspective, this translates to improved ride comfort, reduced lateral acceleration peaks, and enhanced stability; especially under high-speed or uneven-terrain conditions typical of military vehicles.



(a) Front wheel steering angle

(b) Lateral velocity

(c) Yaw rate

(d) XY trajectory for a slalom maneuver

Figure 6. Results with and without the integration of LQR and MPC controllers for a slalom maneuver

In quantitative terms, both controllers significantly reduced tracking errors compared to the open-loop case. For the turning radius maneuver, the RMSE reductions in lateral velocity and yaw rate were 98.2% and 98.4% for MPC, compared to 89.4% and 91.3% for LQR. In the slalom test, where the steering input is smoother than in the previous maneuver, the difference between controllers' response was smaller, yet MPC still achieved lower RMSE values (95.6% and 94.6% against 89.1% and 90.5%, respectively). These results confirm MPC's superior capability for maintaining stability and trajectory precision in the simulations.

However, this improved performance comes at the cost of computational complexity. The MPC requires iterative optimization at each control step, resulting in longer execution time compared to LQR. This trade-off between accuracy and computational cost is a critical consideration for real-time implementation on embedded vehicle platforms. It is also important to highlight that the present study relies solely on simulation results, with experimental data used only for parameter estimation of the proposed SHM. Due to logistical restrictions on testing military vehicles, hardware availability, and safety constraints in field conditions, experimental validation of the proposed controls strategies was beyond the scope of this work. Nevertheless, simulation-based evaluation remains a valid and widely accepted method for early-stage controller assessment.

In order to address this gap, future work could include experimental validation of the proposed algorithms on a scaled or full-size vehicle to verify real-time performance and robustness under realistic conditions. Additionally, future studies may extend the dynamic model and the control algorithms to incorporate a rollover stability index, such as the Load Transfer Ratio (LTR), allowing the controllers to account for rollover risk during aggressive maneuvers. Finally, further enhancements, such as adaptive prediction horizons, dynamic gain tuning, and hybrid model data-driven control strategies represent promising directions to improve real-time performance and robustness, and applicability to advanced driver-assistance systems.

5 Conclusions

This study proposed a trajectory tracking control strategy for a 6×6 armored vehicle based on a simplified dynamic model integrated with LQR and MPC controllers. Parameters estimated from experimental field data were incorporated into the control design to enhance dynamic behavior. Simulation results in MATLAB®/Simulink®, performed under standard maneuvers (turning radius and slalom) demonstrated that the system's key state variables remained within acceptable bounds, indicating that both controllers successfully achieve the intended control objectives while maintaining vehicle stability. However, MPC delivered smoother control actions compared to LQR, which represents a significant advantage for potential real-world applications. Future work should include experimental validation of the proposed controllers on real or scaled vehicles to assess real-time performance. Furthermore, incorporating rollover risk parameters could provide a more comprehensive evaluation of the controllers' effectiveness.

Acknowledgements. The authors would like to thank the Mechanical Engineering Section (SE/4) of the Military Institute of Engineering for providing the resources and support necessary to carry out this work.

Authorship statement. The authors hereby confirm that they are the sole liable persons responsible for the authorship of this work, and that all material that has been herein included as part of the present paper is either the property (and authorship) of the authors, or has the permission of the owners to be included here.

References

[1] Russell, Brett. Development and analysis of active rear axle steering for 8x8 combat vehicle. University of Ontario Institute of Technology (Canada), 2018.
[2] Taghia, Javad; Katupitiya, Jayantha. Applied guidance methodologies for off-road vehicles. Springer International Publishing, 2020.
[3] Acuña MA, Simão Rodrigues G, Queiroz RVG, Lopes EDR. Modeling and dynamic analysis of a 6 x 6 heavy military truck by adaptive model predictive control with application to NATO lane change test course. Proceedings of the Institution of Mechanical Engineers, Part D: Journal of Automobile Engineering. 2020;234(13):3128-3144. doi:10.1177/0954407020924156.
[4] Deng Z, Jin Y, Gao W, Wang B. A closed-loop directional dynamics control with LQR active trailer steering for articulated heavy vehicle. Proceedings of the Institution of Mechanical Engineers, Part D: Journal of Automobile Engineering. 2022;237(12):2741-2758. doi:10.1177/09544070221121859.
[5] Song, W., Min, J., Zhang, T., Zhang, Y., and Zhao, F. Research on Path Tracking Control of Driverless Trucks. In: International Conference on Advances in Construction Machinery and Vehicle Engineering. Singapore: Springer Nature Singapore, 2023. p. 619-632.
[6] Zhang, W.; Wang, J.; Pang, T. Research on the Performance of Vehicle Lateral Control Algorithm Based on Vehicle Speed Variation. World Electric Vehicle Journal. 2025, 16, 259. doi:10.3390/wevj16050259.
[7] Liu X, Liu Z, Gao Q, Guan W. Safe trajectory analysis and validation for multi-axle vehicles considering the stable constraints. Advances in Mechanical Engineering. 2025;17(1). doi:10.1177/16878132251316605.
[8] Jazar, R. N. Vehicle Dynamics, Theory and Application, 3rd ed. Riverdale, NY: Springer, 2014.
[9] Pereira, C. L., da Costa Neto, R. T., and Loiola, B. R. (2021). Cornering stiffness estimation using Levenberg–Marquardt approach. Inverse Problems in Science and Engineering, 29(12), 2207–2238. doi:10.1080/17415977.2021.1910683.
[10] Arndt, M., E. L. Ding, and T. Massel. Identification of cornering stiffness during lane change maneuvers. Proceedings of the 2004 IEEE International Conference on Control Applications, 2004. Vol. 1. IEEE, 2004.
[11] Hu, C.; Wang, Z.; Qin, Y.; Huang, Y.; Wang, J.; Wang, R. Lane keeping control of autonomous vehicles with prescribed performance considering the rollover prevention and input saturation. IEEE Transactions on Intelligent Transportation Systems, IEEE, 2019.
[12] Lin F, Wang S, Zhao Y, Cai Y. Research on autonomous vehicle path tracking control considering roll stability. Proceedings of the Institution of Mechanical Engineers, Part D: Journal of Automobile Engineering. 2020;235(1):199-210. doi:10.1177/0954407020942006.
[13] Ataei, M., Khajepour, A., and Jeon, S. (2018). Model predictive rollover prevention for steer-by-wire vehicles with a new rollover index. International Journal of Control, 93(1), 140–155. https://doi.org/10.1080/00207179.2018.1535198.
[14] Ataei, M., Khajepour, A., and Jeon, S. (2019). Model Predictive Control for integrated lateral stability, traction/braking control, and rollover prevention of electric vehicles. Vehicle System Dynamics, 58(1), 49–73. doi:10.1080/00423114.2019.1585557.
[15] Luty, Witold; Simiński, P. An analysis of cornering stiffness of 14.00 R20 tire with run-flat insert. Journal of KONES, v. 15, p. 295-304, 2008.

[16] Yakub F, Mori Y. Comparative study of autonomous path-following vehicle control via model predictive control and linear quadratic control. Proceedings of the Institution of Mechanical Engineers, Part D: Journal of Automobile Engineering. 2015;229(12):1695-1714. doi:10.1177/0954407014566031.
[17] Pereira, C. L. "Implementação computacional e análise do emprego de um sistema de controle de assistência ao motorista em um modelo de veículo 6x6". Master's degree Thesis, Military Institute of Engineering, 2020.
[18] Durmaz, B. E., Kaçmaz, B., Mutlu, İ., and Söylemez, M. T. Implementation and comparison of LQR-MPC on active suspension system. IEEE. 2017 10th International Conference on Electrical and Electronics Engineering (ELECO). Bursa, TUR, 2017. p. 828–835.
[19] Sánchez, G., Murillo, M., Genzelis, L., Deniz, N., and Giovanini, L. MPC for nonlinear systems: A comparative review of discretization methods. IEEE. 2017 XVII Workshop on Information Processing and Control (RPIC). Mar del Plata, Argentina, 2017. p. 1–6.
[20] Bernardini, Daniele; Bemporad, Alberto. Stabilizing model predictive control of stochastic constrained linear systems. IEEE Transactions on Automatic Control, v. 57, n. 6, p. 1468-1480, 2011.